

Combined Ligand and Structure Guided Design and Virtual Screening of Modulators of Gardos Channel



BILAL QADIR

Master of Science in Bioinformatics

Fall 21-MSBI-NUST00000364861

Supervised by:

Prof. Dr. Ishrat Jabeen

School of Interdisciplinary Engineering & Sciences (SINES)


National University of Sciences & Technology (NUST)


Islamabad, Pakistan

January 2024


THESIS ACCEPTANCE CERTIFICATE

Certified that final copy of MS/MPhil thesis written by Mr. **Bilal Qadir** Registration No.364861 of SINES has been vetted by undersigned, found complete in all aspects as per NUST Statutes/Regulations, is free of plagiarism, errors, and mistakes and is accepted as partial fulfillment for award of MS/MPhil degree. It is further certified that necessary amendments as pointed out by GEC members of the scholar have also been incorporated in the said thesis.

Signature with stamp: 
Name of Supervisor: DR. ISHRAT JABEEN
Professor
School of Interdisciplinary
Engineering & Sciences
Date: 23-01-2024
NUST Sector H-12 Islamabad

Signature of HoD with stamp: 
Date: 25-01-2024
Dr. Fouzia Malik
HoD Sciences
Professor
SINES - NUST Sector H-12
Islamabad

Countersign by

Signature (Dean/Principal): 
Date: 31/01/2024
Dr. Hammad M. Cheema
Principal & Dean
SINES - NUST, Sector H-12
Islamabad

CERTIFICATE OF ORIGINALITY

I hereby declare that the research work presented in this thesis has been generated by me as a result of my own research work. Moreover, none of its contents are plagiarized or submitted for any kind of assessment or higher degree. I have acknowledged and referenced all the main sources of help in this work.

Bilal Qadir

Fall 2021-MS BI 00000364861

Dedication

This dissertation is dedicated to my parents Mr. and Mrs. Ghulam QADIR, my Supervisor Dr. Ishrat Jabeen, my teachers for their endless love, guidance, support, encouragement and invaluable belief in me.

ACKNOWLEDGEMENTS

I begin by expressing my heartfelt gratitude to Allah, I am deeply thankful for His support in helping me to accomplish my goal of obtaining my MS degree. A special note of appreciation goes out to my dedicated teachers who have been instrumental in shaping my academic path. I am profoundly indebted to my supervisor, *Dr. Ishrat Jabeen*. Her unwavering support, expert guidance, and endless patience have been my guiding lights during moments of research challenges. Her mentorship has not only enriched my academic pursuits but also nurtured my growth as a researcher. I extend my sincere gratitude to the esteemed members of my guidance committee: *Dr. Uzma Habib, Dr. Masood ur Rehman Kayani*. Your thoughtful insights and encouraging words have played a crucial role in refining my research and shaping my academic perspective.

It is with deep gratitude that I turn to my family, who have been my unwavering pillars of support for me. My mother stands as the epitome of selflessness and determination. All credit goes to her. Her sacrifices and boundless encouragement have paved the way for all of my accomplishments throughout my career. To my father, whose love and guidance inspire me.

Finally, I extend my gratitude to all those who, in ways both seen and unseen, have contributed to my academic and personal growth. May the knowledge I have gained and the accomplishments I have achieved stand as a testament to the collective efforts that have shaped my path.

BILAL QADIR.

Table of Contents

Abstract.....	12
Chapter 1.....	14
Introduction.....	15
1.1. Structure of Gardos Channel.....	16
1.2. Distribution of Gárdos Channel.....	17
1.3. Gating mechanism of KCNN4.....	17
1.4. Normal and Diseased KCNN4 Channel.....	18
1.5. KCNN4 as a Drug Target.....	20
1.6. Mutations and Modulators of KCNN4 Channel.....	20
1.7. Challenges.....	21
1.8. Problem Statement.....	21
1.9. Proposed Strategy.....	22
1.10. Novelty of work.....	22
1.11. Objectives.....	22
Chapter 2.....	23
Literature Review.....	24
2.1. Channel Activity.....	25
2.2. Structural analysis of Gárdos Channel.....	25
2.3. Relation between KCNN4 wild type and R352H mutant.....	26
2.4. Relation between KCNN4 and V282M/E mutant.....	27
2.5. Inhibitors of Gardos Channel.....	27
Chapter 3.....	29
Methodology.....	30
3.1. Collection of datasets.....	30
3.2. Pharmacophore Model 1.....	30
3.3. Pharmacophore Model 2.....	30
3.4. Molecular Docking of Known Data.....	31
3.5. Pharmacophore Model Evaluation.....	32
3.6. Virtual Screening.....	32
3.7. GRIND (Grid-Independent molecular descriptor).....	32
3.8. Molecular Docking of Hits.....	33
3.9. Molecular Dynamics Simulation.....	33
Chapter 4.....	34
Results.....	35

4.1.	Collection of datasets	35
4.2.	Pharmacophore Model 1	42
4.3.	Pharmacophore Model 2	43
4.4.	Molecular Docking of Known Data	45
4.5.	Pharmacophore Model Evaluation	46
4.6.	Virtual screening	46
4.7.	GRIND (Grid-Independent molecular descriptor)	47
4.8.	Molecular Docking of Hits.....	48
4.9.	Molecular Dynamics Simulation.....	52
Chapter 5	55
Discussion	56
Chapter 6	57
Conclusion	58
Chapter 7	60
References	61

LIST OF FIGURES

Figure 1: Graphic topology of the Gardos Channel in cell membrane.	16
Figure 2: Structure and membrane topology of KCNN4 at calmodulin binding domain.	18
Figure 3: Mechanism and effects observed in normal and mutated KCNN4 in RBCs.	19
Figure 4: Mutations pointed out in Gardos Channel structure.	21
Figure 5: Ion transport pathway of potassium distribution in the red cells.	25
Figure 6: KCNN4 crystal structure representing the 4 chains and 4CaM domains.	26
Figure 7: Docking protocol used to dock known data at calmodulin binding domain.	31
Figure 8 Mutant Model of Gardos Channel retrieved from previous data.	35
Figure 9: 2D image of Pharmacophore model	42
Figure 10: 3D image of pharmacophore model	43
Figure 11 : The top active ligand Gardos_43_3561 selected as template	44
Figure 12: 3D image of pharmacophore model developed which is Gardos_43_3561.	44
Figure 13: Top ligand Interactions in binding pocket of protein.	45
Figure 14 : Molecular weight and LogD of Hits	47
Figure 15 : Compound 1 forming interactions in binding pocket of protein.	49
Figure 16: Compound 2 forming interactions in binding pocket of protein.	49
Figure 17: Compound 3 forming interactions in binding pocket of protein.	50
Figure 18 : Compound 4 forming interactions in binding pocket of protein.	50
Figure 19 : Compound 5 forming interactions in binding pocket of protein.	51
Figure 20: This figure represents interactions formed at final frame of MD Simulation	53
Figure 21: Output obtained after the Molecular Dynamic Simulation of top hit with	53
Figure 22: Output obtained after the Molecular Dynamic Simulation of top hit with	54

List of Tables

Table 1: X, Y and Z coordinates for Calmodulin binding domain around R352 mutation	31
Table 2: 2D structure of ligands dataset retrieved from previous data.	36
Table 3 Distances calculated between features of pharmacophore.	42
Table 4: Pharmacophore features and distances in-between	43
Table 5 : Comparison of model's evaluation	46
Table 6 : Predicted IC50 of top 10 hits	48

List of Equations

Equation 1 : Mathematical Equation of GoldScore Function	31
Equation 2 : GRIND Model Equation	33

List of Abbreviations

KCNN4, KCa3.1	Intermediate Conductance calcium channel, Gardos Channel
HX	Hereditary Xerocytosis
MCHC	Mean Corpuscular Hemoglobin concentration.
R352H	Arginine352Histidine
V282M	Valine282Methionine
V282E	Valine282Glutamic acid
DRY	Hydrophobic
O	Hydrogen Acceptor
NI	Hydrogen Donor
TIP	Shape Based feature.
VSMC	Vascular smooth muscle cells
REST	Repressor element-1 silencing transcription factor
AP-1	Activator protein 1
EF-hands	Helix-loop-helix
CAMBD	Calmodulin binding domain
CaM	Calmodulin binding domain
WT	Wild Type
NHE	Na ⁺ /H ⁺ exchanger
NKCC	Na-K-Cl cotransporter
PTH	Parathyroid hormone
PGE-2	Prostaglandin E2
Cryo-EM	Cryo-electron microscopy
PDB	Protein databank
MMFF94X	Merck Molecular Force Field
MOE	Molecular Operating Environment
CSC	Common scaffold clustering
QSAR	Quantitative Structural Activity Relationship
GRIND	GRID Independent Descriptors
CLACC	Consistently large and auto cross-correlation

GOLD	Genetic optimization and ligand binding
HBA	Hydrogen Bond Acceptor
HBD	Hydrogen Bond Donor
PLS	Partial least square analysis
ARO HYD	Aromatic and Hydrogen

Abstract

Red Cell deformability refers to the ability of red blood cells (erythrocytes) to change their shape to pass through narrow capillaries and small vessels in the circulatory system. In red cell deformability, an abnormality can result in impaired blood flow and decreased oxygen delivery, which can contribute to a variety of diseases such as Sickle cell anemia and hereditary xerocytosis. The Gardos Channel, also known as the calcium-activated potassium Channel (KCNN4/KCa3.1), is found in the membrane of red blood cells. In diseased conditions, hyperactivation of the Gardos Channel allows potassium ions to exit the cell, which leads to water loss and reduces the volume of the cell. In previous studies, Gardos Channel has been identified as a potential drug target because of its role in regulating red Cell volume. Inhibition of the Gardos Channel has been shown to increase the hydration of cells and maintain their normal shape which can be beneficial for diseases of red cell deformability. Previously, a structure- guided protocol was opted to explore the binding hypothesis of Gardos Channel (KNCC4) which could facilitate the design of the KNCC4 modulators. Three-point mutations R352H, V282M and V282E have been identified previously in Gardos Channel which subsequently led to the development of Senicapoc, Clotrimazole, Tram-34, UCL 1684 and 1-EBIO drugs. However, none of these drugs showed efficacy against reported mutations. Therefore, in this study, a combined ligand and structure-guided protocol was opted for virtual screening of modulators of Gardos Channel. The protocol consists of building ligand-based pharmacophore models, molecular docking, model evaluation, virtual screening, GRIND analysis, docking of hits and Molecular dynamic simulation. The data of known ligands of Gardos Channel and the mutant model of Gardos Channel was retrieved from the literature. Two types of pharmacophore models were developed in this study. The docking of 50 known ligands was done at the Calmodulin binding domain of Gardos Channel, generating an internal database for model evaluation. Virtual screening of unknown drug data was performed using the final selected pharmacophore model. The GRIND analysis was used for the prediction of IC_{50} values of hits. The predicted IC_{50} values for the top five hits fall within the range of 5.85nM to 12.67nM. The top five compounds with the highest IC_{50} values were docked at the Calmodulin binding domain, and a Molecular Dynamic simulation of the top pose of the highest active compound was carried out to probe the stability. The molecular dynamics simulations result showed the presence of residues MET282, ALA297, ARG287, TYR199, LEU198 and VAL195 within vicinity of ligand. The presence of MET282 and ALA297 is important as they formed a hydrophobic pocket, thus providing optimal fit of ligand and MET282 is one of our target mutations. This compound exhibits superior interactions with the

target, as no previously identified ligand has demonstrated interactions with the specific point mutation. The predicted IC_{50} of this compound is 5.85nM while the IC_{50} of the top active compound from known data is 8.99nM, therefore it has better binding potential against the Gardos channel than the already known compound. The Lipophilic efficiency value of this compound is 7.47 which qualifies the FDA criteria of an average oral drug.

Chapter 1

Introduction

Introduction

The **Gardos Channel** is a cation channel also referred to as KCNN4 or KCa3.1. It is a Calcium-activated, potassium channel, expressed in many cell types including erythrocytes [1]. It plays a key role in regulating ion flow and cell volume through its activation in response to intracellular calcium levels. The channel activation is linked to intracellular calcium concentrations, allowing control over potassium ion movement and maintaining cellular homeostasis. The abnormal activity of Gardos Channel in erythrocytes is characterized by an abnormal cation leak resulting in KCl loss and red blood cell dehydration. Dehydration leads to cell weakness and hemolytic anemia [2].

In this disease "hemolytic anemia", a slit-like shape is deformed with abnormal membrane permeability to the monovalent cations such as Na⁺ and K⁺. These monovalent cations are responsible for the osmotic stability of the cell [3]. The abnormal membrane transport was also first recognized in the hereditary stomatocytosis disease of humans. Among these diseases, **Hereditary xerocytosis (HX)** is the most common variant [4].

In hereditary xerocytosis, red blood cells exhibit an abnormally reduced volume and a characteristic cup shape. In HX patients, red blood cells show altered intracellular cation content and cellular dehydration, which are responsible for an increased erythrocyte hemoglobin concentration and a decreased erythrocyte osmotic fragility [5]. In this condition, there is excessive dehydration of red blood cells. The changed shape and less flexibility of the dehydrated red blood cells destroy of the spleen.

Hereditary xerocytosis is caused by mutations in genes that encode ion channels and transporters involved in regulating the movement of ions across the red blood cell membrane. Mutations in different genes are associated with the condition, including the PIEZO1, KCNN4, and ABCB6 genes [6].

The Gardos Channel is also an important therapeutic target for **sickle cell disease (SCD)**. SCD is a genetic disorder characterized by the presence of abnormal hemoglobin (hemoglobin S), which causes red blood cells to become rigid and take on a sickle shape under certain conditions. This altered shape and rigidity of red blood cells contribute to vascular events, pain, tissue damage, and other complications.

1.1. Structure of Gardos Channel

The structure of Gardos Channel is a **homo-tetramer** of six transmembrane domains (S1-S6) which is predicted from its amino acid sequence [7]. The region between the s5 and s6 membrane domains contains the pore region [8]. The potassium selectivity is mediated by the carbonyl oxygen atoms within the selectivity filter coming out from the backbone of the polypeptides from each of the four identical subunits [9]. It contains two membrane-spanning α -helices and one RCK (regulator of conductance of K^+) domain per subunit. To form a channel, four subunits unite in the presence of four additional RCK domains from the solution. It shows that the binding of Ca^{2+} refers to a conformational change in the cytoplasmic 'gating ring' of eight RCKs, which translates to bringing changes in the arrangement of α -helices in the pore which makes the channel open [10]. In steady-state conditions, Gardos Channel is inactive. Under specific conditions, intracellular Ca^{2+} increases and interacts with Calmodulin molecules that are bound tightly on each of the four subunits of the Gardos Channel. Ca^{2+} binding to Calmodulin results in the opening of the channel and rapid K^+ and Cl^- efflux, leading to erythrocyte dehydration and shrinkage [4].

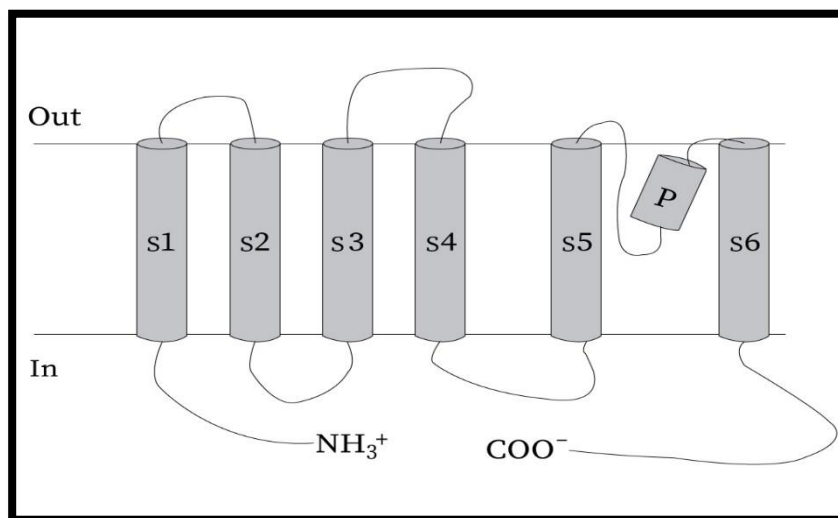


Figure 1: Graphic topology of the Gardos Channel in cell membrane.[7, 11]

1.2. Distribution of Gárdos Channel

Gardos Channel is expressed in erythrocytes, smooth muscle cells, T lymphocytes, macrophages and other cells linked with thrombotic disorders [12]. It is also found in hematopoietic system cells, as well as salt and fluid-transporting organs (including colon, lung, and salivary glands). Platelets, lymphocytes, mast cells, monocytes/macrophages, epithelial tissues (gastrointestinal, lung, endocrine glands, exocrine glands), vascular endothelial cells, vascular smooth muscle cells (VSMC), and fibroblasts are all known to expressed by the KCa3.1 channel [13].

1.3. Gating mechanism of KCNN4

In the gating mechanism and channel activation, the structure of the KCNN4 combined with Calcium ion concentration plays a vital role [14]. The Calmodulin-binding domain initiates the gating mechanism. Calmodulin (CAM) consists of two lobes (N- and C- lobe), each containing two pairs of helix-loop-helix (EF-hand) motifs [15]. The EF-hands are the binding sites for Calcium ions. There are four binding sites for Calcium ions within the cell. These binding sites are numbered from I to IV from N-terminus, the binding sites require calcium binding at the high closeness to initiate conformation modification in the structure-directing to gate activation [16, 17].

The homology model of the channel reveals that Calmodulin C-lobe ties in a calcium-independent manner to a region on the c-terminal tail of the channel. called the Calmodulin-Binding domain 1, while the N-lobe ties in a calcium-dependent manner, to the Calmodulin-Binding domain 2A of one subunit and Calmodulin-Binding domain 2B of the lateral subunit. This interaction introduces modifications in Calmodulin and the S6 transmembrane leading towards a change in pore structure and opening of the gate[18]. Data from recent studies also reveal that residues present in the pore and transmembrane region could activate and close the channel. Among them, the F248 residue of the pore region interacts with the W216 residue of the S5 transmembrane to stabilize the closed conformation of KCNN4. Similarly, F248 may interact with residue G274; located near the gating hinge on the S6 helix, to stabilize the open state of KCNN4[19, 20] .

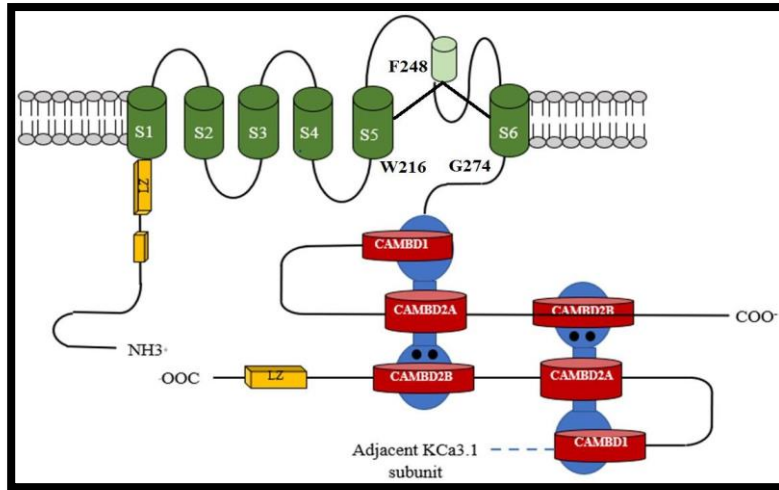


Figure 2: Structure and membrane topology of KCNN4 at calmodulin-binding domain.

1.4. Normal and Diseased KCNN4 Channel

Under normal conditions, due to Ca^{2+} influx in the cell, the Gárdos channel activates and hyperpolarizes the membrane of red cells towards the K^{+} equilibrium potential by the efflux of K^{+} ions, thus amplifying the signal transduction. Also, a more active Gárdos channel constantly leaks the K^{+} ions and water, resulting in cell shrinkage as represented in Fig 3. In the case of the mutated KCNN4, the K^{+} leak is followed by cell shrinkage that leads to a K^{+} influx through Na-K-Cl cotransporter (NKCC) [21]. The $\text{Na}^{+}/\text{H}^{+}$ exchanger (NHE) activity is enhanced which increases the NKCC-mediated Na^{+} accumulation in the cell. Abnormal Na^{+} concentration results in cell swelling, leading towards Na, K-ATPase activation, and energy consumption (decreased ATP and enhanced stimulation of glycolysis). The research using flow cytometry and cell imaging techniques revealed the Ca^{2+} overload in the cell, which might be due to the activation of the PIEZO1 channel (possibly activated due to cell swelling) or Ca^{2+} entry pathways [22].

This increased concentration further activates the KCNN4 and the cycle continues, leading towards a premature removal of RBS from the circulation. In my opinion, controlling the Ca^{2+} concentration in the cell with mutated KCNN4 can help in reducing the cause.

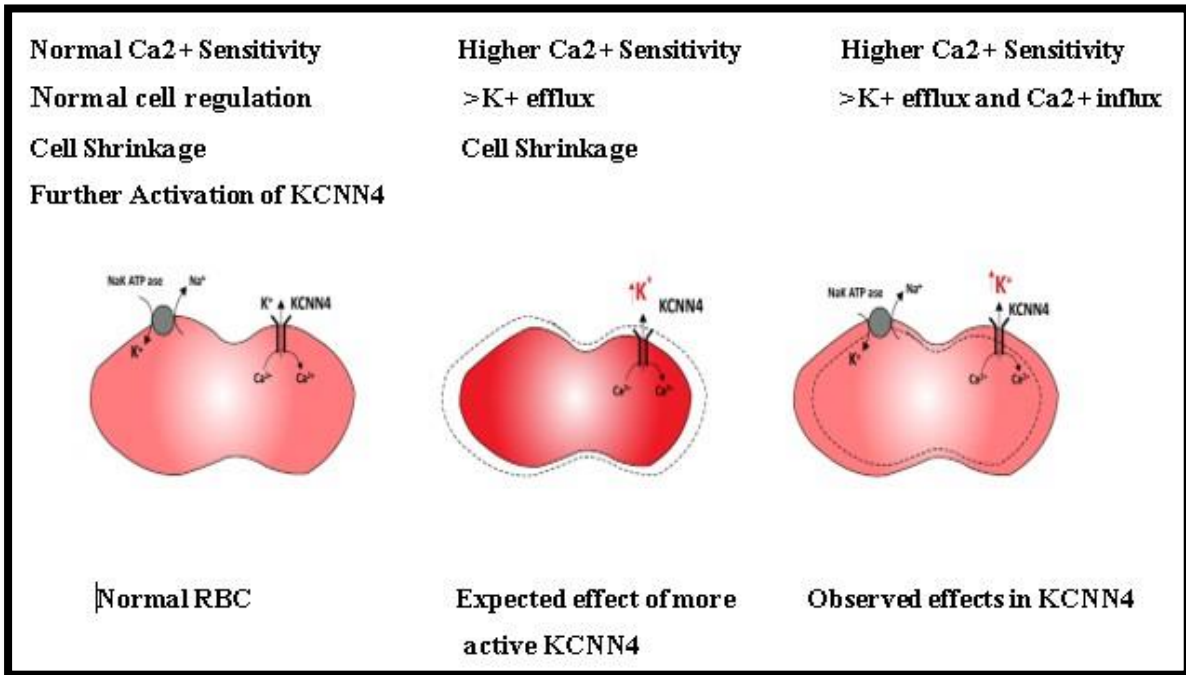


Figure 3: Mechanism and effects observed in normal and mutated KCNN4 in RBCs[23]. In hyperactivated KCNN4, higher Ca²⁺ sensitivity is observed leading to K⁺ leak causing cell shrinkage.

1.5. KCNN4 as a Drug Target

The Gárdos channel with the support of regulating cell membranes and calcium signal is involved in erythrocyte volume regulation, lymphocyte activation, macrophage migration, vascular smooth muscle cell and fibroblast proliferation, and other processes, leading towards a crucial role in the development of various diseases [4]. The Gardos Channel blocking can lead to the treatment of various diseases. Gardos Channel blockers can regulate cell volume and shape. Clotrimazole, TRAM-34 and ICA-17043, which block KCNN4, reduce cancer cell proliferation in vitro [24]. As a result, KCNN4 channel blockers slow tumor development [25]. Drugs that block the KCNN4 channel or gene knockouts of the KCNN4 channel can alleviate renal fibrosis caused by bilateral ureteral obstruction [26]. KCNN4 channel blockers could be utilized to treat chronic kidney disease caused by hypertension or diabetes [27]. TRAM-34, a KCa3.1 channel blocker developed by Wulff *et al.* [28] in 2000, has a substantial blocking effect and no clear adverse liver reaction. It's commonly employed in animal and cell research experiments. TRAM-34 has the benefit of being extremely selective. TRAM-34 does not alter the cell activity of human T lymphocytes, VSMC, macrophages, or endothelial cells [29]. Its blocking effect on KCa3.1 channel is more than 1000 times that of other potassium, sodium, and calcium channels.

1.6. Mutations and Modulators of KCNN4 Channel

Gardos Channel is a tetramer of 4 identical subunits, encoded by the KCNN4 gene. Mutations at two different amino acid residues in KCNN4 (R352H, V282M/E) are reported in patients from 6 independent families with dehydrated hereditary stomatocytosis which are shown in Figure 4 [30]. These mutations can be seen in Figure 4. In recent studies aimed at studying the effect of the Gardos Channel inhibitor Senicapoc, it is observed that the three mutants result in higher channel activity, although they do not share a common mechanism in altering channel characteristics, i.e. Ca²⁺ sensitivity. However, the link of the *Gardos Channel* dysfunction to increased hemolysis has so far not been elucidated [31]. Numerous drugs such as Senicapoc, clotrimazole and TRAM-34 have been designed to block the activity of the Gárdos channel, but none of them are completely efficient against all three mutations.

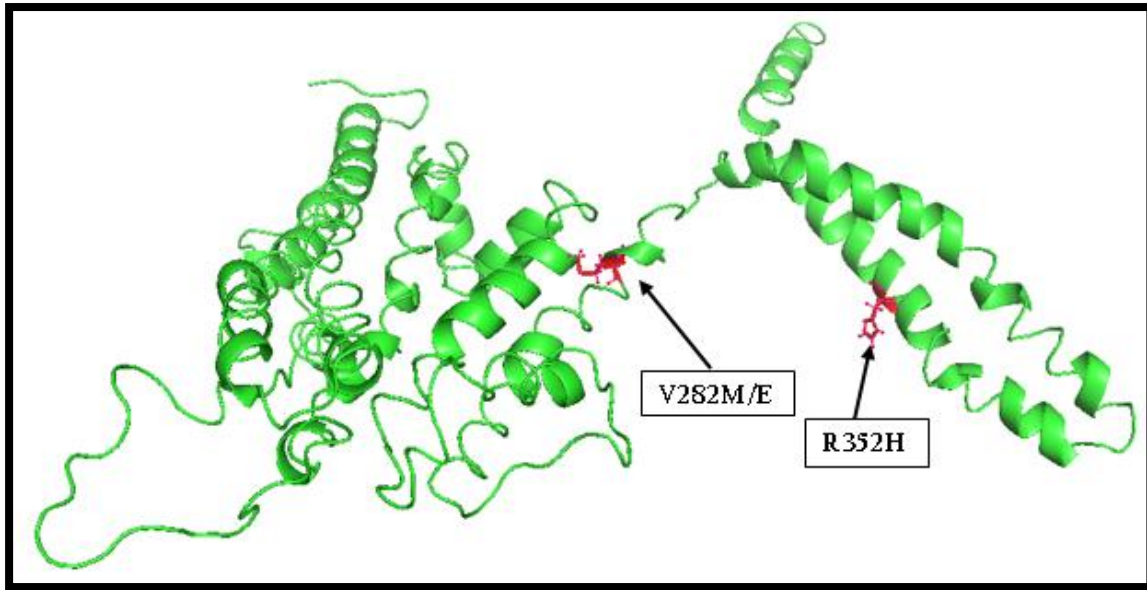


Figure 4: Mutations pointed out in Gardos Channel structure.

1.7. Challenges

Due to the unavailability of the X-ray crystal structure of the KCNN4 till 2018, there was no structural analysis available. There was no analysis for designing modulators for this channel. Thus, in the present project, ligand and structure-guided design of modulators and virtual screening was done with the help of a mutant model of this channel built in previous project [32].

1.8. Problem Statement

Ca²⁺ Presence of certain hereditary mutations in the Gárdos channel, makes the channel less sensitive to Ca²⁺ therefore, these gain-of-function mutations in CAMBD of the Gárdos channel, associated with Ca²⁺ influx, K⁺ efflux, and dehydration can be controlled by either targeting the transmembrane domain and completely blocking the activation of the Gárdos channel, or modulating the mutant CAMBD and making it less sensitive to intracellular Ca²⁺ by various drug-like entities, thus maintaining a stable Ca²⁺ gradient inside and out of the cell. This could help avoid the premature death of red cells. Investigating the allosteric sites in the Calmodulin binding domain of mutated KCNN4 can also deliver requisite results.

1.9. Proposed Strategy

This study proposes ligand and structure-guided design of modulators and virtual screening of modulators of KCNN4 channel for its normal physiological function so that it can maintain cell shape and volume which is considered the root of the whole problem.

1.10. Novelty of work

The already-designed modulators of KCNN4 are effective against one or two types of mutation. The drugs are not effective against all three types of mutations. We aim to design a drug effective against all mutations which is never done before.

1.11. Objectives

The following are objectives of this research:

- 1.11.1** To develop a virtual screening protocol for the design and screening of the modulators of the KCNN4
- 1.11.2** Validation of the identified hits against KCNN4 using Molecular Dynamic simulations of ligand-protein complexes.

Chapter 2

Literature Review

Literature Review

The **Gárdos Channel** is a Ca^{2+} sensitive, K^{+} selective Channel found in several tissues, where it is involved in Cell volume regulation. Mutations at two different amino acid residues in KCNN4 are reported in patients with hereditary xerocytosis in a study [33]. It is identified by whole exome sequencing a new family with two members affected by chronic hemolytic anemia carrying mutation R352H in the KCNN4 gene. No additional mutations in genes encoding for red blood cells cytoskeletal, membrane or Channel proteins are detected. Functional studies were performed on patients to evaluate the effects of R352H mutation on the Cellular properties and eventually on the clinical phenotype. The Gárdos Channel hyperactivation is observed in circulating erythrocytes. The '**Gárdos Channelopathy**' is a complex pathology and it is difficult to modulate such complex Channelopathy [23].

Hereditary xerocytosis (HX) is caused by mutations in either the mechanosensitive cation Channel PIEZO1 or the Ca^{2+} -activated K^{+} Channel KCNN4. All HX-associated KCNN4 mutants studied to date have shown increased current magnitude and red Cell dehydration. KCNN4 activity is increased in HX red Cells heterozygous for KCNN4 mutant V282M. However, wild-type cation contents on HX red Cells failed to restore wild-type-stimulated KCNN4 activity to those HX Cells. The chronic KCNN4-driven red Cell dehydration and intracellular cation imbalance can lead to reduced KCNN4 activity in HX [17].

It is observed that two different genes are linked to this disease which are PIEZO1, specifically coding for a non-selective cation Channel and Gárdos Channel in RBCs [34]. Among the 3 KCNN4 mutations linked to Hereditary Xerocytosis, one is in the Calmodulin-binding (CaMB) domain (*R352H*) whereas the two others are **V282M and V282E**, affect the same residue in the pore domain. It is observed that R352H substitution in the CaM domain changes the Ca^{2+} threshold for activation. It increases current density and delays Channel inactivation. The Gárdos Channel hyperactivity results in the loss of K^{+} and water. Whereas V282 residue plays a key role in KCNN4 gating, however, the way how these substitutions(*V282M/E*) affect Channel functioning in the pore domain is not observed [35].

2.1. Channel Activity

Since the first reports of Ca^{2+} -activated K^+ permeability in erythrocytes, several "measures" have been proposed to describe K^+ fluxes as being caused by the Gárdos channel. For example, the need for calcium at the intracellular face of the channel ($(\text{Ca}^{2+})_i$); a single-channel conductance of 20 pS (at 0 mV); high selectivity of K^+ over Na^+ ; evidence of open channel inward rectification; gating independence of membrane potential; inhibition either by specific drugs such as clotrimazole and charybdotoxin; or inhibition on pre-incubation of cells in the absence of external potassium ($(\text{K}^+)_o$) [36]. These identification criteria can and have been modulated through different physiological and experimental conditions.

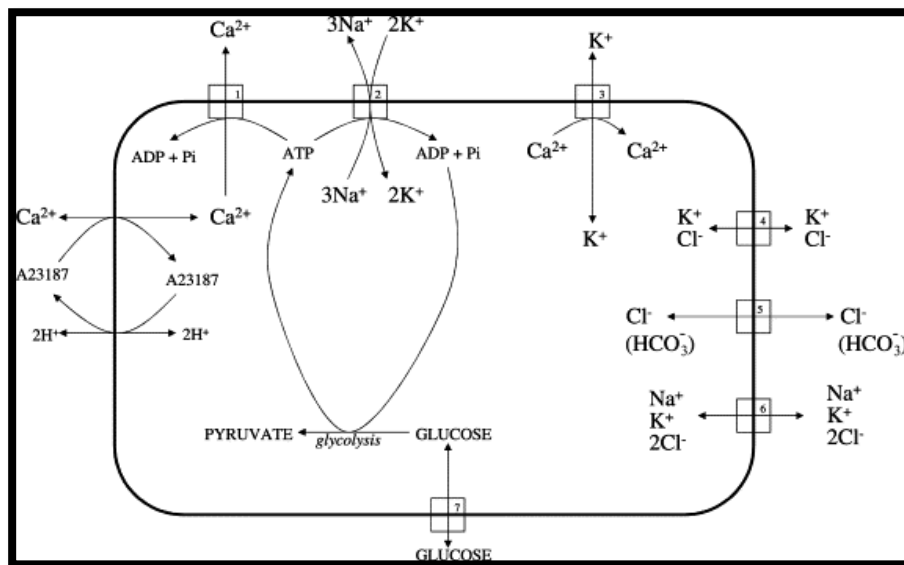


Figure 5: Ion transport pathway of potassium distribution in the red cells.

2.2. Structural analysis of Gárdos Channel

In 2018, a study done by Chia-Hsueh Lee and Roderick MacKinnon helped in the demonstration of cryo-electron microscopy (cryo-EM) structures of a human **SK4-CaM** channel complex (KCNN4) in a closed and open state at a resolution of 3.4 – 3.5 Angstrom [37]. In KCNN4, four Calmodulin (CaM) molecules were attached. (Fig. 5) The CaM had two distinct lobes. Each lobe of the **CaM** was associated with a distinct function. The C-lobe of CaM binds to the channel, whereas the N lobe was involved in the interaction between the S4-S5 linker in a calcium-dependent manner. The S4-S5 linker is composed of two distinct helices [38]. When the CaM molecule binds, these helices undergo conformational changes, leading towards an open state of the channel. The

structure of KCNN4 published in 2018, revealed the basis for understanding the pharmacology of the KCNN4 channel [39].

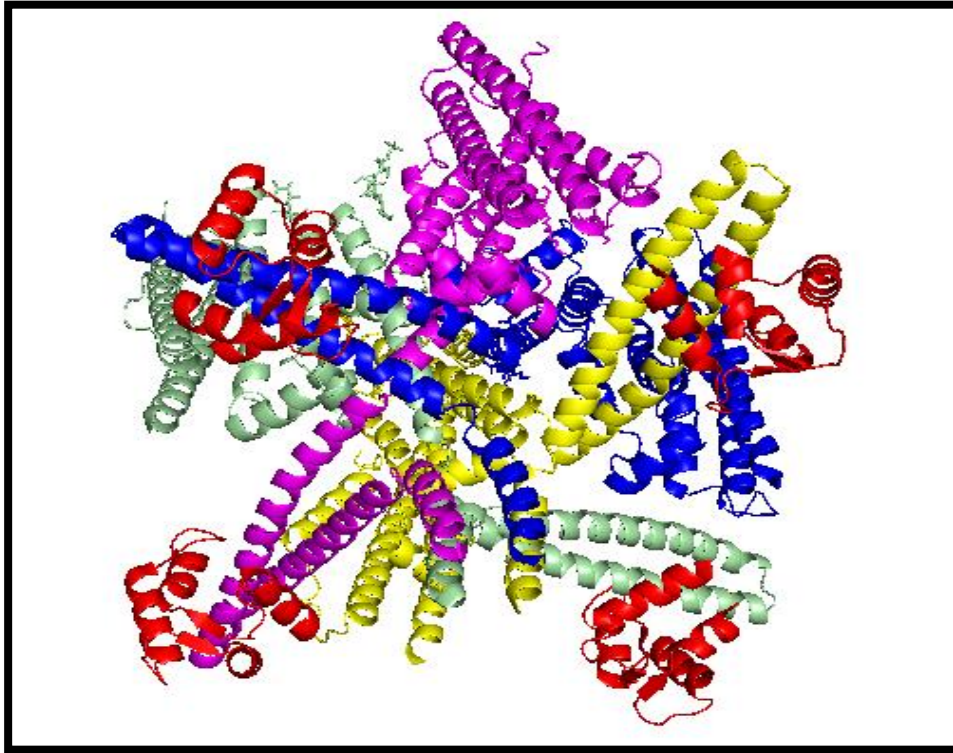


Figure 6: KCNN4 crystal structure representing the 4 chains and 4CaM domains. Each chain is represented in a different color and CaM is represented in red color.

2.3. Relation between KCNN4 wild type and R352H mutant

Experimentation and studies of some researchers helped in elucidating the crucial role of R352 in channel activation through Calmodulin interaction. Firstly, the research by Schumacher et al, demonstrating the crystal structure of Calmodulin bound to the **calmodulin-binding domain** in KCNN2 (another calcium-dependent potassium channel), the residue Arginine at the 464 position in the calmodulin-binding domain was found to interact with glutamine at position 84, present in the C- lobe of calmodulin aiding in the calcium-independent interaction between the calmodulin molecule and the domain [40]. Coinciding with this research, the Arg464 residue may correspond to the Arg352 in KCNN4 [41]. Secondly, the research by Morales et al, presented a significant contribution to the gating mechanism of KCNN4 through the KCNN4-calmodulin interaction process. The research stated that during the gating process, electrostatic interaction occurs between the Arg352 of one monomer of KCNN4 and the Glu363 of the adjacent monomer of KCNN4. This interaction

then contributes to the open probability of the Gárdos channel [18]. In the same model, it was also observed that the substitution of Arg352 by Cysteine resulted in an increased deactivation time for the Gárdos channel. Thus, it may be possible that the substitution of mutant residue Histidine in place of Arg352 may change electrostatic interactions with Glu363, leading towards a change in kinetic properties of KCNN4 and thus a prolonged activation of Gárdos channel for p. Arg352His mutant [42].

2.4. Relation between KCNN4 and V282M/E mutant

V282M mutation in KCNN4 is directly linked with the disease Hereditary xerocytosis. It was proved in a study done by Edyta Glogowska et al. in 2015. It was confirmed in their study by segregation analysis that transmission of the KCNN4 mutation with disease phenotype is present in affected individuals [43]. These mutations were not present in non-HX family members. These mutations were both predicted to be pathogenic by PolyPhen2, a tool used in the prediction of the impact of an amino acid substitution on the structure and function of proteins using required considerations, SIFT, and other mutation prediction tools. The mutations were present both in conserved residues, with highly significant phastCons(hidden Markov model-based method, based on the multiple alignment used to predict the probability that each nucleotide belongs to a conserved element) scores of 1.0 for both V282M and V282E and highly significant PhyloP(useful to predict the signs of selection at a particular nucleotide or classes of nucleotides)conservation scores (V282M 7.489 and V282E 8.923) [44]. These amino acids are highly conserved across vertebrate species, including the clades of placental mammals, the extant Eutherians, and members of the small-intermediate family of calcium-activated potassium channels [45].

2.5. Inhibitors of Gardos Channel

Several inhibitors of the Gárdos Channel, also known as KCa3.1, have been developed and tested for their efficacy in treating various diseases, including Sickle Cell disease, asthma, and autoimmune disorders. Senicapoc is a small molecule inhibitor of the Gárdos Channel that has been shown to reduce red blood Cell dehydration and sickling in patients with Sickle Cell disease [46]. Senicapoc has been tested in clinical trials and showed promising results in reducing the frequency of painful crises and the need for blood transfusions in patients with Sickle Cell disease [47] [48].

Charybdotoxin (CTX) is a peptide toxin that has been identified from the venom of the scorpion

Leiurus quinquestratus. CTX is observed to inhibit the Gárdos Channel with an IC₅₀ value of 100 pM [49].

UCL 1684 is a small molecule inhibitor of the Gárdos Channel that has been identified through high-throughput screening. The reported IC₅₀ value of UCL 1684 is 160 nM [50].

1-EBIO is a small molecule activator of the Gárdos Channel that has been shown to have biphasic effects on Channel activity, acting as an inhibitor at high concentrations. The reported IC₅₀ value of 1-EBIO as an inhibitor of the Gárdos Channel is 9.8 μM [50].

TRAM-34 is another small molecule inhibitor of the Gárdos Channel which is tested in preclinical studies and has shown efficacy in reducing hyperresponsiveness. TRAM-34 has also been shown to have immunosuppressive effects and is being investigated as a potential treatment for autoimmune disorders [47].

Based on our current understanding of the molecular pathogenesis of Sickle Cell disease, several independent treatment approaches have been proposed to date, however, the only available cure is allogeneic bone marrow transplantation, a form of therapy that is limited by the availability of potential donors and by toxicity. Hydroxyurea, the one drug that has been approved by the Food and Drug Administration specifically for the treatment of severe SCD, decreases the frequency of painful events, acute chest syndrome, and requirements for blood transfusions. Many Hydroxyurea-treated SCD patients continue to experience vaso-occlusive complications, develop end-organ damage, require a blood transfusion, and exhibit life expectancies that remain substantially decreased compared with healthy individuals [51].

Chapter 3

Methodology

Methodology

3.1. Collection of datasets

A dataset of ligands and mutant model of Gardos Channel was obtained from previous data [52]. The mutant model of Gardos Channel was not available, so it was generated with added mutations utilizing homology modeling previously [52]. The original structure of Gardos Channel was obtained from PDB (Protein Data Bank) ID 6CNM. The mutant model structure was validated through Molecular Dynamic simulations. The ligand dataset of 56 compounds with known IC₅₀ was originally obtained from the ChEMBL database from known literature. After filtering and removal of duplicates, 51 compounds were finalized for study [52]. A dataset of 55622 unknown compounds was retrieved from the ChemBridge database for virtual screening.

3.2. Pharmacophore Model 1

Pharmacophore models have proved to be very useful for identifying important features of ligands and receptors of protein. The two major types of pharmacophore modeling are structure-based pharmacophores and ligand-based pharmacophores. Structure-based pharmacophores are obtained directly from X-ray structures of protein and ligand complexes while ligand-based pharmacophores are obtained from structures of known active compounds. A ligand-based pharmacophore model was generated using an efficient tool LigandScout 4.4.8 for better understanding features within our dataset of ligands. LigandScout builds models based on active and common features within ligands.

3.3. Pharmacophore Model 2

The dataset of 51 known ligands of KCNN4 protein was retrieved from previous data. The top ligand of data was selected as a template for building pharmacophore model. The other 50 ligands in data were left for evaluation of the pharmacophore model which consisted of 25 actives and 25 inactive reported from literature. The template was selected based on the highest activity value and flexibility of a compound. The template was first pre-processed, and energy was minimized using Molecular Operating Environment Version 2015. A pharmacophore model was built on a template by selecting 5 main features. These features were later tuned to give the best outcome.

3.4. Molecular Docking of Known Data

The mutant model of KCNN4 protein structure and dataset of 50 known compounds were pre-processed using MOE (Molecular Operating Environment) version 2015. Ligands were energy minimized and a force field of MMFF94x was selected. Protein was protonated in 3D; errors were corrected. Ligands were then docked at the Calmodulin binding domain of the KCNN4 protein where R352 mutation occurs. The docking process was carried out through the GOLD tool (Genetic Optimization for Ligand Docking) 5.6.1 version. The binding pocket was selected through adjustment X, Y and Z axis coordinates around the Calmodulin binding domain. A radius of 27 angstroms was set to select all active residues within the binding pocket. For each ligand, a sum of 250 genetic runs was performed by using GoldScore to rank the resulting poses of each ligand using the Gold Scoring function as equation 2:

$$\Delta G (bind) = \Delta G (hb_ext) + \Delta G (vdw_ext) + \Delta G (hb_int) + \Delta G (vdw_int)$$

Equation 1 : Mathematical Equation of GoldScore Function

Early termination was allowed for ligands. All other parameters were set to default and slow protocol was set to achieve more precision and accuracy. Table 1 shows the X, Y and Z coordinates selected for the Calmodulin binding domain. Figure 7 shows the general workflow of this docking protocol.

Table 1: X, Y and Z coordinates for the Calmodulin binding domain around the R352 mutation

Region	Coordinates for active binding site		
	X	Y	Z
Calmodulin binding domain	140	139	140

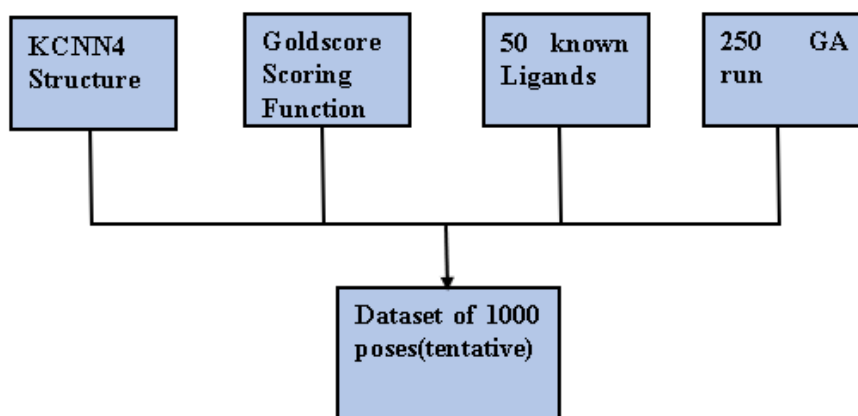


Figure 7: Docking protocol used to dock known data at the calmodulin-binding domain

3.5. Pharmacophore Model Evaluation

The internal database constructed by docking 50 compounds at the Calmodulin binding domain was packed for evaluation of both pharmacophore models. It was reported from the literature that compounds having more than 7.02 IC₅₀ values are active and less than 6.4 IC₅₀ values are inactive. This threshold defines that 25 compounds are active and 25 are inactive. The internal database of conformations generated by the docking process was used to evaluate the selection ability of the pharmacophore model in discerning active compounds from inactive compounds. The database screening for evaluation of pharmacophore model 1 was carried out using the pharmacophore searching available in LigandScout software. The database screening for evaluation of pharmacophore model 2 was carried out using the pharmacophore searching available in MOE software.

3.6. Virtual Screening

To find effective inhibitors of Gardos Channel, the ChemBridge database of 55622 molecules was used for virtual screening because of the diverse structures of compounds. These 556222 compounds had a total of 348063 conformations which were packed for screening. Based on the generated pharmacophore model, the search protocol for the pharmacophore of the MOE was used to screen hits from the ChemBridge database. This pharmacophore model selected those compounds out of data that exactly mapped with pharmacophore features of the model.

3.6.1. Computation of 2D descriptors

A web-based tool ADMETLab 2.0 (Absorption, Distribution, Metabolism, Excretion, Toxicity) was used to compute 2d descriptors of hits. LogD and molecular weight of compounds were observed. Hits were screened through golden triangle to check potency of drug candidates.

3.7. GRIND (Grid-Independent molecular descriptor)

The data set of 51 known ligands with their known IC₅₀ values was loaded in the software Pentacle v1.07 to calculate Grid Independent Descriptors. GRIND are alignment-free molecular descriptors, connected with 3D structural conformations of the dataset. A GRIND model was developed using the given data. This model used 4 probes which are DRY (Hydrophobic), N1 (Hydrogen bond donor), O (Hydrogen bond acceptor) and TIP (Molecular shape) to calculate MIF (Molecular Interaction Fields). GRIND model predicted IC₅₀ values of unknown data (Hits) using known molecular conformations and IC₅₀ values of known data.

Total energy at each point was computed as the sum of Lennard-Jones (Elj), electrostatic (Eel), and hydrogen bond (Ehb) as described in Equation (1) by iteratively placing each probe at different GRID steps.

$$E_{xyz} = \Sigma E_{lj} + \Sigma E_{el} + \Sigma E_{hb}$$

Equation 2 : GRIND Model Equation

3.8. Molecular Docking of Hits

After predicting IC50 values of hits using the GRIND model, the top 10 compounds with high IC50 values were selected for docking. Docking was done to analyze the binding interactions of hits. All molecules were docked at the Calmodulin binding domain near the R352H residue. For each ligand, a sum of 100 genetic runs was performed by using GoldScore to rank the resulting poses of each ligand. The protocol was set the same as done before for generating conformations of known data explained in Molecular Docking (3.4).

3.9. Molecular Dynamics Simulation

Molecular dynamics (MD) simulations are carried out using the software GROMACS 3.3.3 package with the standard GROMOS96 force field. The top complexes of docking outcome were used in this process. The water molecules, heteroatoms and unwanted molecules were removed from the PDB file of complexes. In preparation, missing sidechains and atoms were added using pdb2gmx (a GROMACS utility). TIP3P was used to add solvent. The system was neutralized by adding counter ions (e.g., Na⁺ or Cl⁻) to achieve the desired ionic concentration using the genion tool in GROMACS. The energy minimization was done to remove steric clashes and reduce potential energy by using the steepest descent or conjugate gradient algorithms in GROMACS. The system was equilibrated to have the desired pressure and temperature using GROMACS mdrun. Simulation was run for 200 nanoseconds with a TIP3P solvent model to get the stable structure.

Chapter 4

Results

Results

4.1. Collection of datasets

A mutant model of the Gardos Channel was retrieved from previous data shown in Figure 8. A total of 51 known modulators of the Gardos Channel were retrieved from previous data and originally retrieved from the ChEMBL database. A database of 55622 unknown compounds was retrieved from the ChemBridge database.

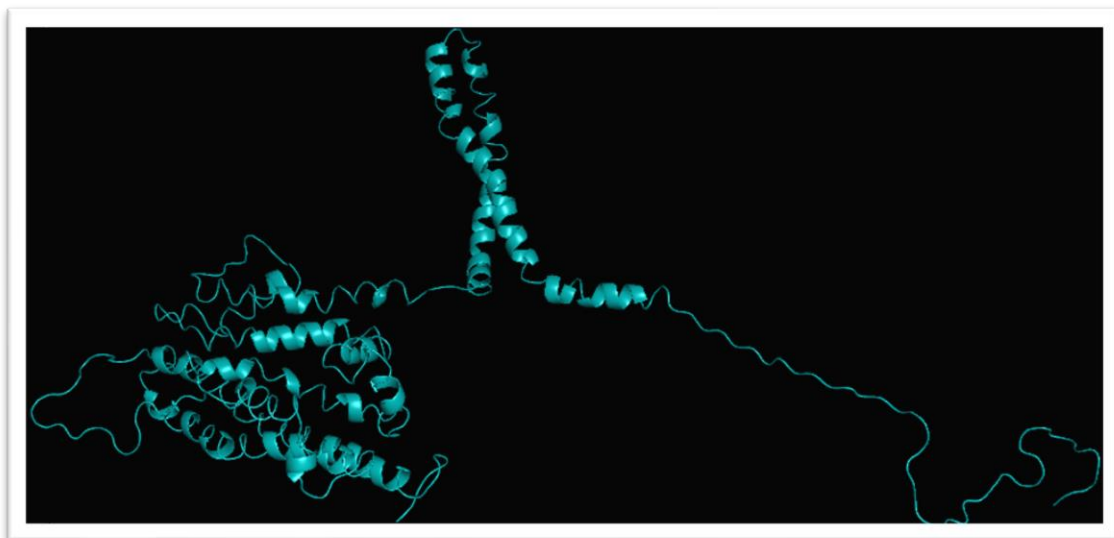
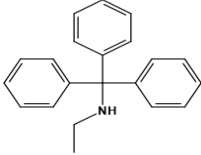
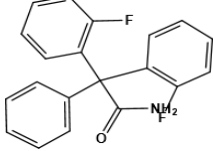
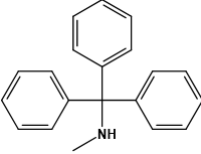
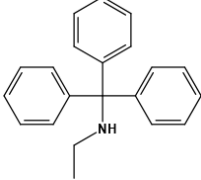
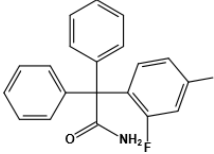
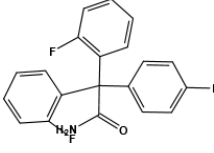
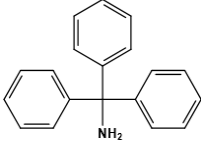
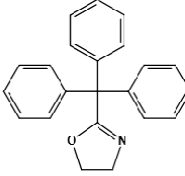
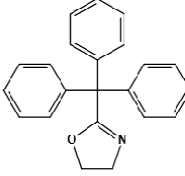
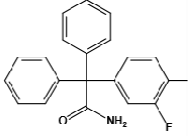
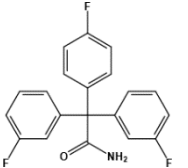
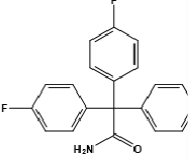
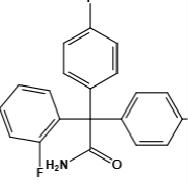
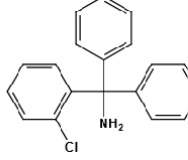
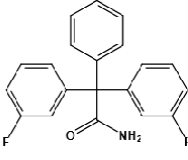
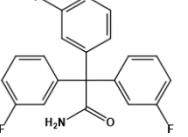
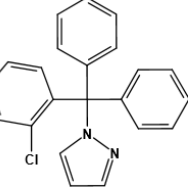
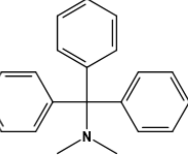
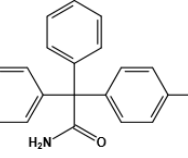
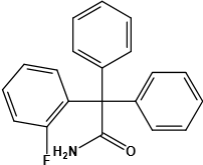
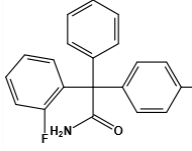
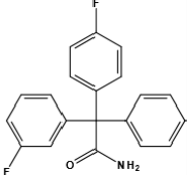
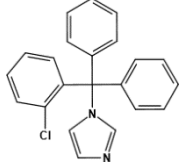
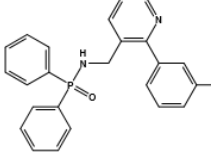
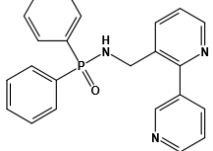
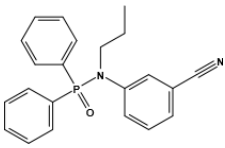
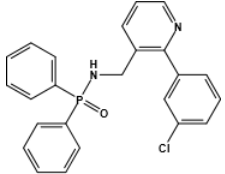
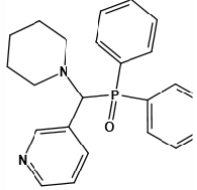


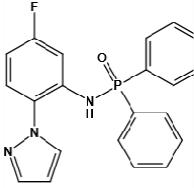
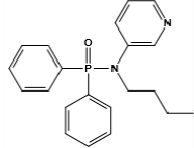
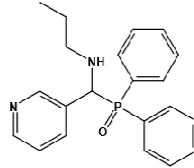
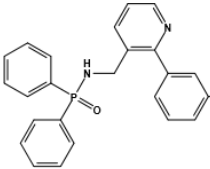
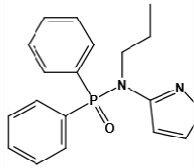
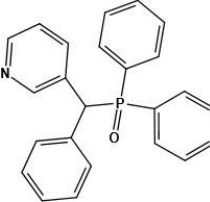
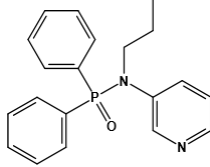
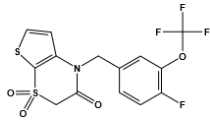
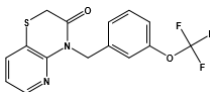
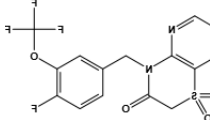
Figure 8 Mutant Model of Gardos Channel retrieved from previous data[52]

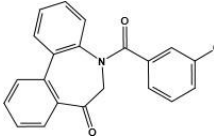
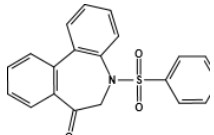
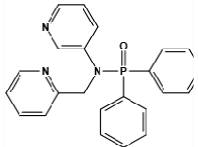
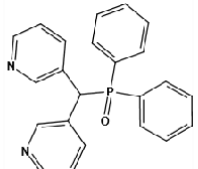
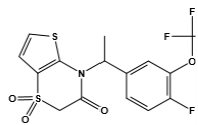
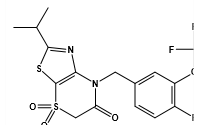
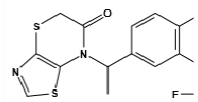
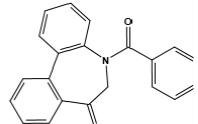
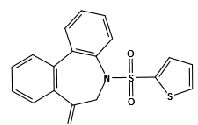
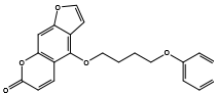
Table 2: 2D structure of ligands dataset retrieved from previous data. [52]

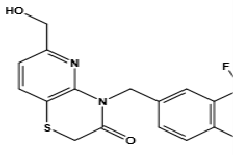
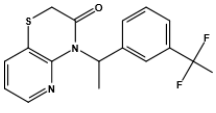
Sr no	ChEMBL ID	2D Structure
1	Gárdos_1	
2	Gárdos_2	
3	Gárdos_3	
4	Gárdos_5	
5	Gárdos_6	
6	Gárdos_7	
7	Gárdos_8	
8	Gárdos_21	
9	Gárdos_22	

10	Gárdos_26	
11	Gárdos_29	
12	Gárdos_30	
13	Gárdos_37	
14	Gárdos_38	
15	Gárdos_39	
16	Gárdos_42	
17	Gárdos_12	
18	Gárdos_13	
19	Gárdos_14	

20	Gárdos_17	
21	Gárdos_43	
22	Gárdos_49	
23	Gárdos_18	
24	Gárdos_11	
25	Gárdos_15	
26	Gárdos_16	
27	Gárdos_19	
28	Gárdos_40	

29	Gárdos_44	
30	Gárdos_45	
31	Gárdos_46	
32	Gárdos_20	
33	Gárdos_47	
34	Gárdos_34	
35	Gárdos_35	
36	Gárdos_4	
37	Gárdos_9	
38	Gárdos_23	

39	Gárdos_27	
40	Gárdos_28	
41	Gárdos_48	
42	Gárdos_51	
43	Gárdos_24	
44	Gárdos_33	
45	Gárdos_50	
46	Gárdos_36	
47	Gárdos_41	
48	Gárdos_10	

<p>49</p>	<p>Gárdos_31</p>	
<p>50</p>	<p>Gárdos_25</p>	

4.2. Pharmacophore Model 1

Model 1 was generated by using known data on inhibitors of Gardos Channel. Structures of 51 ligands were given to the software LigandScout version 4.4.8. The model generation parameter was set to 5 and all other parameters were set to default. Five models were generated based on common features between ligands. Each model was developed having four common features which are H1, H2, Aromatic and Hydrogen Bond Acceptor. Features distances are shown in Table 3. 2D and 3D model images are shown in Figure 9 and 10 respectively.

Table 3 Distances calculated between features of pharmacophore.

Features	Distances
HBA – H1	3.66A
HBA – Aromatic	3.34A
HBA – H2	4.6A
H1 – Aromatic	0.33A
H1 – H2	5.91A
Aromatic – H2	5.67A

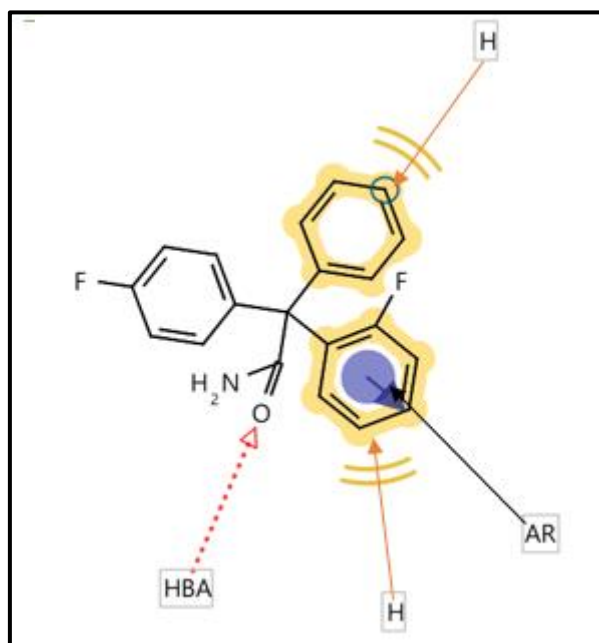


Figure 9: 2D image of Pharmacophore model

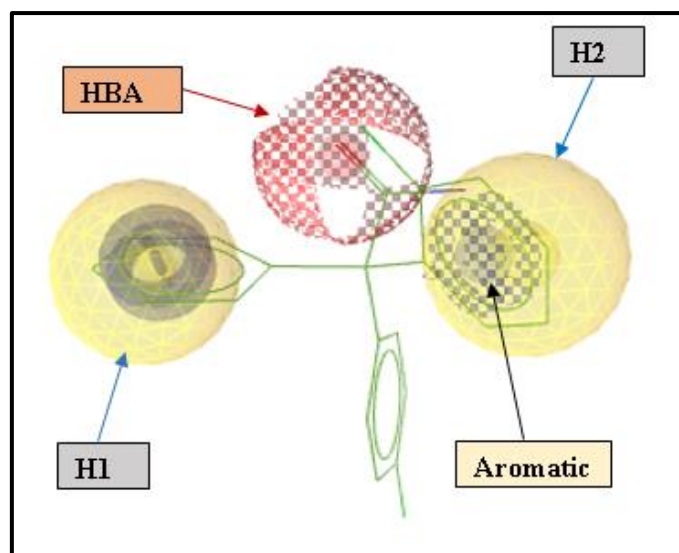


Figure 10: 3D image of pharmacophore model

4.3. Pharmacophore Model 2

Model 2 was generated by the software Molecular Operating Environment version 2015. The highest active ligand from known data was selected as a template. Five active features were selected for template which are F1 Aromatic and Hydrophobic, F2 Aromatic and Hydrophobic, F3 Aromatic and Hydrophobic, HBA and HBD. Selected features and distances computed between them are shown in Table 4. The template is shown in Figure 11. Pharmacophore model with selected features is shown in Figure 12.

Table 4: Pharmacophore features and distances in-between

Features	Distances
F1 Aro Hyd - F2 Aro Hyd	5.16A
F1 Aro Hyd - F3 Aro Hyd	4.85A
F1 Aro Hyd – HBA	4.07A
F1 Aro Hyd – HBD	5.36A
F2 Aro Hyd - F3 Aro Hyd	5.29A
F2 Aro Hyd – HBA	4.89A
F2 Aro Hyd – HBD	3.78A
F3 Aro Hyd – HBA	4.67A
F3 Aro Hyd – HBD	4.38A
HBA – HBD	2.23A

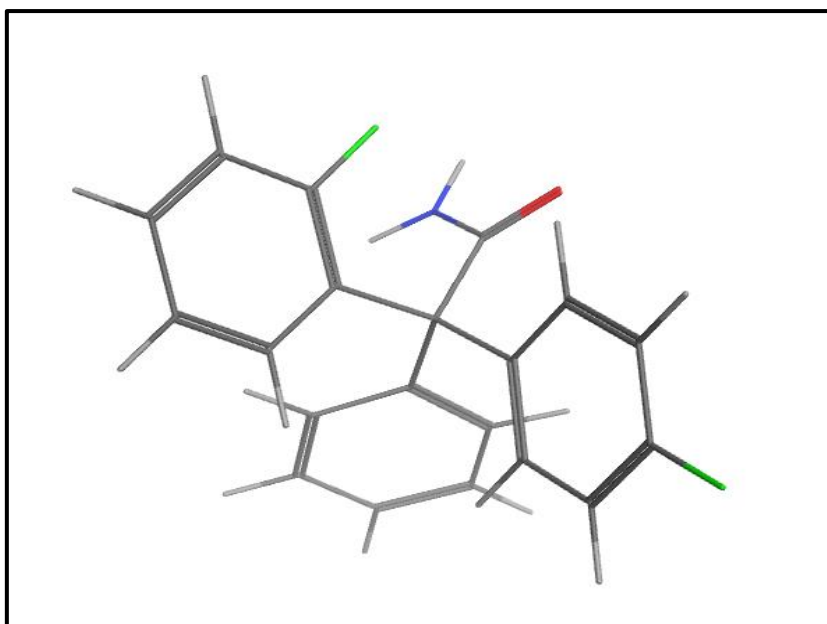


Figure 11 : The top active ligand Gardos_43_3561 selected as template

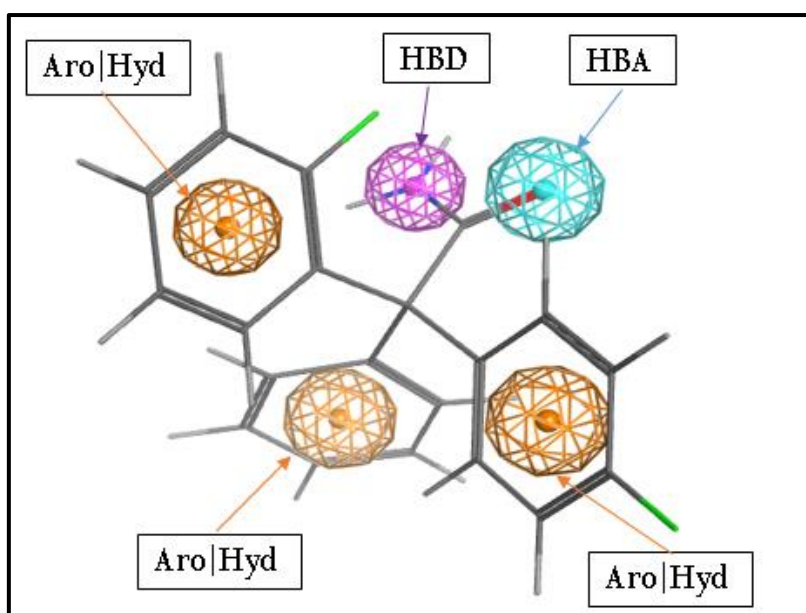


Figure 12: 3D image of pharmacophore model developed on template which is Gardos_43_3561.

4.4. Molecular Docking of Known Data

Molecular docking is the most effective approach in molecular modeling for modeling atomic-level interactions between proteins and ligands. It enables the understanding of fundamental biological processes by analyzing the behavior of chemical compounds in the target protein's binding region. The goal of molecular docking is to acquire the most probable confirmation of ligands for virtual screening. Using a crystal structure of the mutant model of KCNN4(PDB ID: 6CNM) with a resolution power of 3.40 Å, a dataset of 50 ligands was docked into the binding pocket of the calmodulin-binding domain. All the important amino acid residues were included in the binding site, which was kept at a radius of 20Å. The GOLD scoring function was used to rank each pose of docked ligands. Early termination was allowed for protocol. All other parameters were set to default and slow protocol was set to achieve more precision and accuracy. For 50 ligands, a total of 3085 poses were generated.

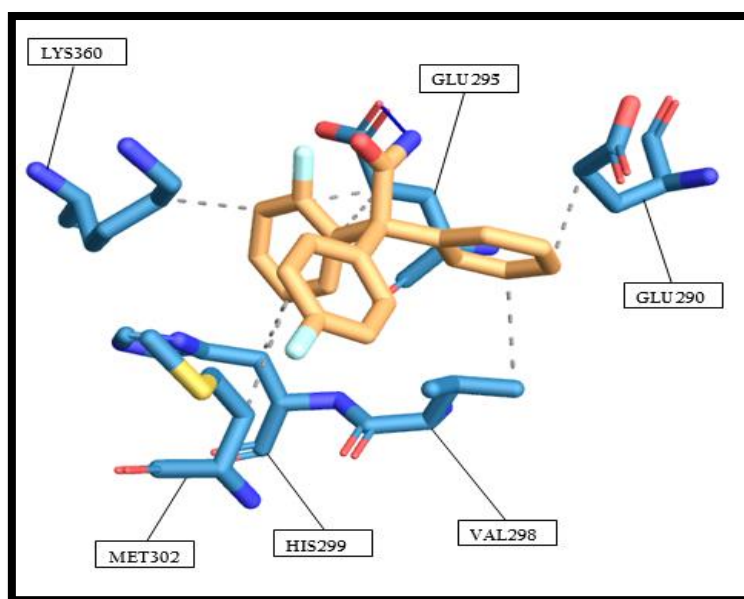


Figure 13: Top ligand Interactions in the binding pocket of the protein.

4.5. Pharmacophore Model Evaluation

The internal database constructed by docking was packed for evaluation of the pharmacophore model. It was reported from the literature that compounds having more than 7.02 IC₅₀ values are active and less than 6.4 IC₅₀ values are inactive. This threshold defines that 25 compounds are active and 25 are inactive. The screening of the internal database was carried out to evaluate the selection ability of the pharmacophore model in discerning active compounds from inactive compounds. The database screening for evaluation of pharmacophore model 1 was carried out using the pharmacophore searching available in LigandScout software. The database screening for evaluation of pharmacophore model 2 was carried out using the pharmacophore searching available in MOE software.

Table 5 : Comparison of model's evaluation

Measures	Model 1(LigandScout)	Model 2(MOE)
Accuracy	0.6111	0.7600
Precision	0.6667	1.000
Sensitivity	0.3200	0.5200
Specificity	0.8621	1.0000
F1 Score	0.4324	0.6842

Model 2 outperformed Model 1 in the evaluation of precision metrics. Model 2 was selected for virtual screening.

4.6. Virtual screening

The ChemBridge database of 55622 molecules was used for virtual screening because of the diverse structures of compounds. These 55622 compounds had a total of 348063 conformations which were packed for screening. Pharmacophore model 2 was selected in model evaluation so, the search protocol for pharmacophore in the MOE tool was carried out to screen hits from the ChemBridge database. This pharmacophore model selected 312 hits from a database of 55622 compounds.

4.6.1. Computation of 2D descriptors

A web-based tool ADMETLab 2.0 (Absorption, Distribution, Metabolism, Excretion, Toxicity) was used to compute 2d descriptors of hits. LogD and molecular weight of compounds were observed. Hits were screened through a golden triangle to check potency of drug candidates. All drugs passed through this criterion of standardized Molecular weight and logD.

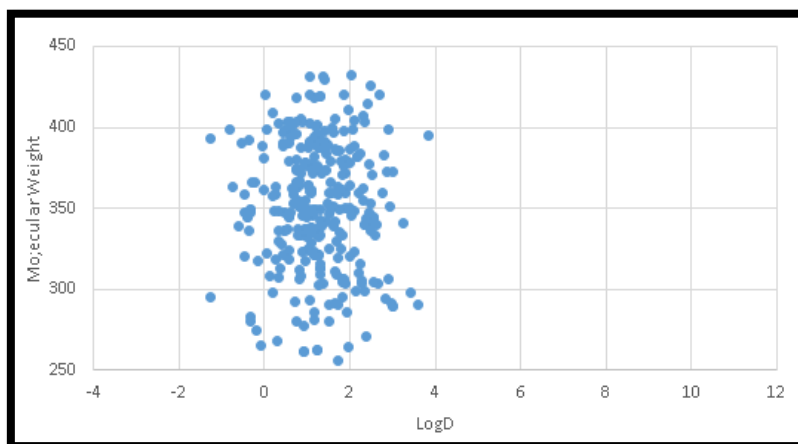
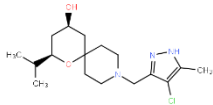
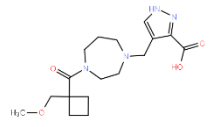
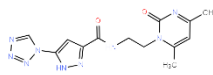
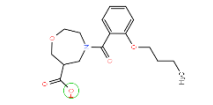
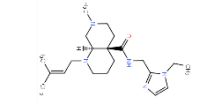
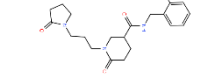
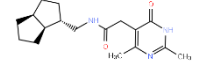
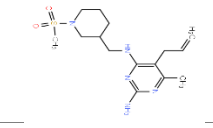
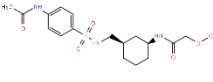
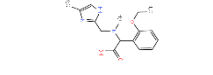


Figure 14 : Molecular weight and logD of Hits

4.7. GRIND (Grid-Independent molecular descriptor)

The data set of 51 known ligands with their known IC₅₀ values was loaded in the software Pentacle v1.07 to calculate Grid Independent Descriptors. GRIND are alignment-free molecular descriptors, connected with 3D structural conformations of the dataset. A GRIND model was generated using the given data. This model used 4 probes which are DRY (Hydrophobic), N1 (Hydrogen bond donor), O (Hydrogen bond acceptor) and TIP (Molecular shape) to calculate MIF (Molecular Interaction Fields). GRIND model predicted IC₅₀ values of unknown data (Hits) using known molecular conformations and IC₅₀ values of known data. The predicted PIC₅₀ values of the top 10 hits are shown in Table 6.

Table 6 : Predicted PIC₅₀ of top 10 hits

Compound ID	2D Structures	Predicted PIC ₅₀
<i>1</i>		8.23274
<i>2</i>		8.00248
<i>3</i>		7.99843
<i>4</i>		7.90254
<i>5</i>		7.90258
<i>6</i>		7.89706
<i>7</i>		7.66249
<i>8</i>		7.55126
<i>9</i>		7.45932
<i>10</i>		7.20426

4.8. Molecular Docking of Hits

After predicting IC₅₀ values of hits using the GRIND model, the top 5 compounds with high IC₅₀ values were selected for docking. Docking was done to analyze the binding interactions of hits. All molecules were docked at the **Calmodulin binding domain** near the R352H residue. For each ligand, a sum of 100 genetic runs was performed by using GoldScore to rank the resulting poses of each ligand. The protocol was set the same as done before for generating conformations of known data explained in the methodology of Molecular Docking (3.4). These top 5 hits showed common interactions. Binding Interactions of these top 5 hits are shown in the figures below.

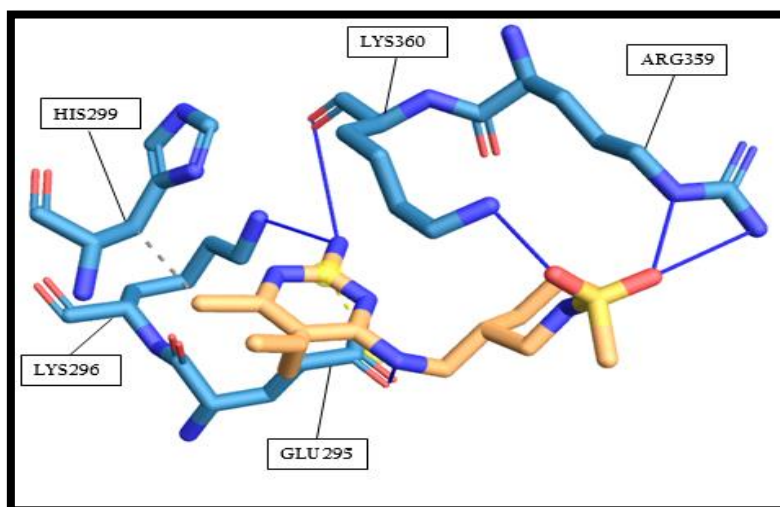


Figure 15 : Compound 1 forming interactions in the binding pocket of the protein.

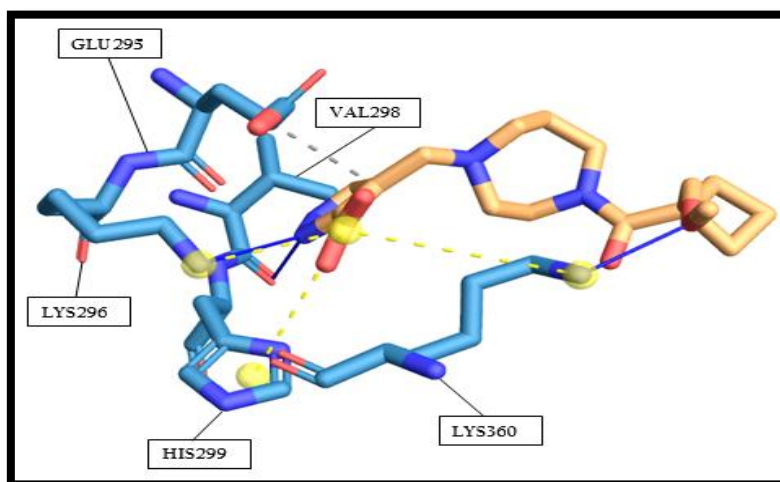


Figure 16: Compound 2 forming interactions in the binding pocket of the protein.

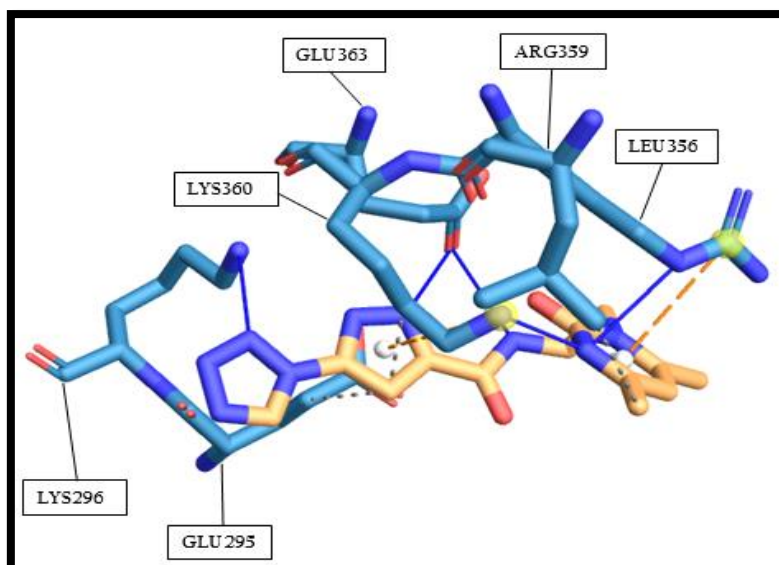


Figure 17: Compound 3 forming interactions in the binding pocket of the protein.

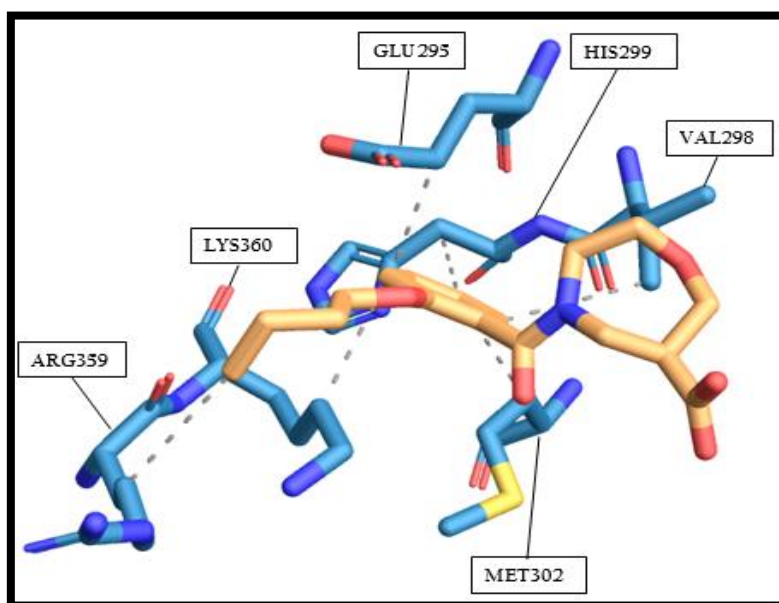


Figure 18 : Compound 4 forming interactions in the binding pocket of the protein.

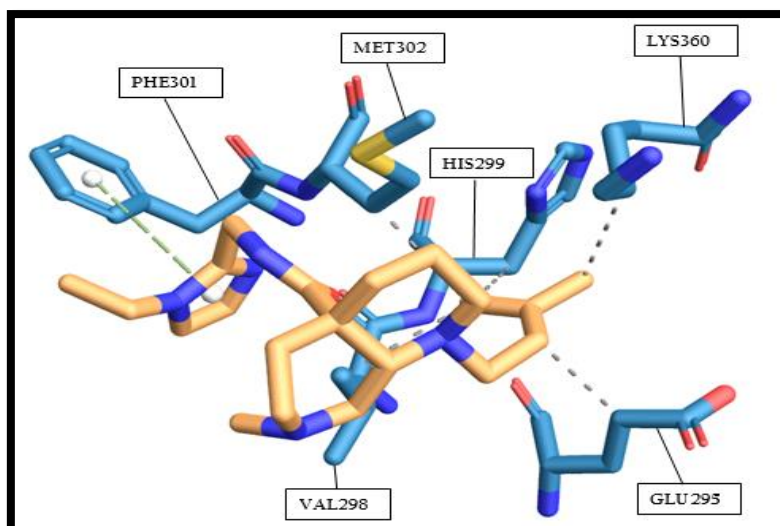


Figure 19 : Compound 5 forming interactions in the binding pocket of the protein.

4.9. Molecular Dynamics Simulation

The complex underwent a molecular dynamic simulation, lasting 200ns at a pH value of 7.4. The simulation duration was extended due to the presence of loops at the structure's beginning and end. Stabilization occurred at the 200ns mark, attributed to the existence of these loops. To prepare, water molecules, heteroatoms, and undesired molecules were eliminated from the PDB file of complexes. Missing sidechains and atoms were then added using `pdb2gmx`, a utility in GROMACS. Solvent (TIP3P) was used, and the system's neutrality was achieved by adding counter ions (e.g., Na⁺ or Cl⁻) to attain the desired ionic concentration through the `genion` tool in GROMACS. Energy minimization, employing steepest descent or conjugate gradient algorithms in GROMACS, was performed to eliminate steric clashes and decrease potential energy. Subsequently, the system underwent equilibration to reach the desired pressure and temperature using GROMACS `mdrun`. The molecular dynamics simulations result showed the presence of residues MET282, ALA297, THR278, TYR199, LEU198 and VAL195 within vicinity of ligand as shown in Figure 20. The presence of MET282 and ALA297 is important as they formed a hydrophobic pocket, thus providing optimal fit of ligand and MET282 is one of our target mutations. The RMSD and RMSF graph for this simulation is showed in Figure 21 and Figure 22 respectively. This compound exhibits superior interactions with the target, as no previously identified ligand has demonstrated interactions with the specific point mutation. The predicted IC₅₀ of this compound is 5.85nM while the IC₅₀ of the top active compound from known data is 8.99nM, so it is much better than the already known compound. The Lipophilic efficiency value of this compound is 7.47 which qualifies the FDA criteria of an average oral drug.

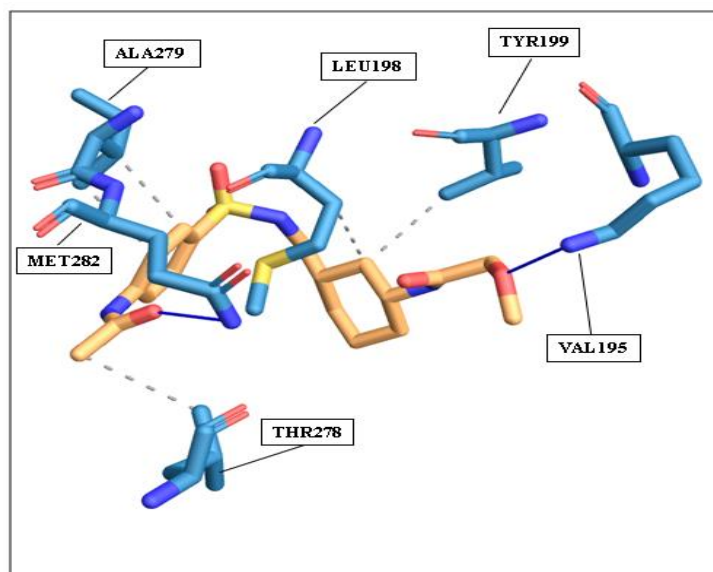


Figure 20: This figure represents ligand interactions formed with protein at final frame of Molecular dynamic Simulation.

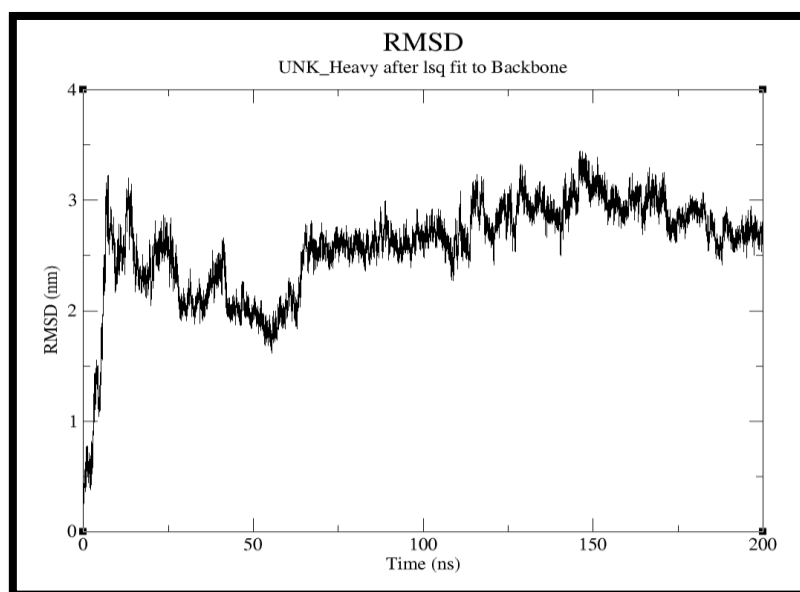


Figure 21: Output obtained after the Molecular Dynamic Simulation of top hit with modeled mutant KCNN4 structure. The graph shows RMSD values (y-axis) vs. time(ns) (x-axis).

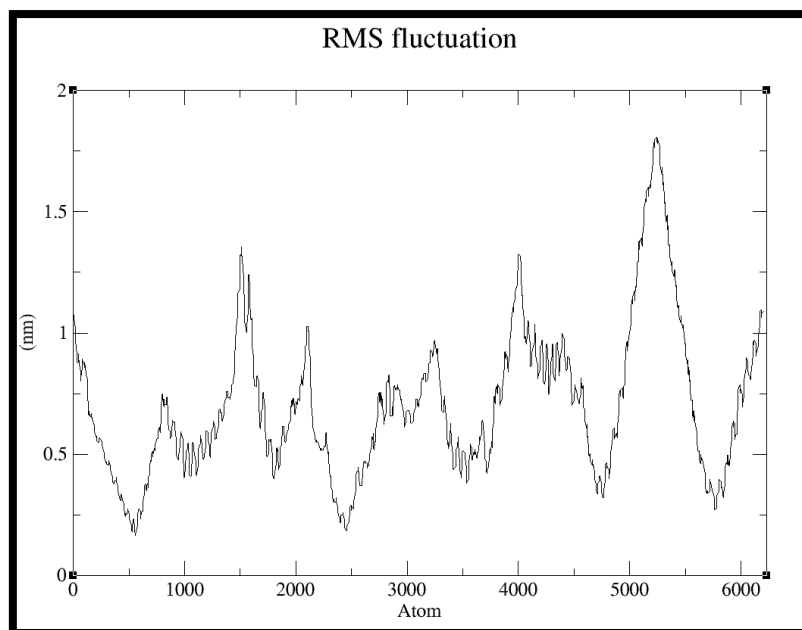


Figure 22: Output obtained after the Molecular Dynamic Simulation of top hit with modeled mutant KCNN4 structure. The graph shows RMSF values (y-axis) vs. Residue Index (x-axis).

Chapter 5

Discussion

Discussion

There is no solution to stop the spread of hereditary diseases, however, the treatment of such diseases is possible by the administration of drugs and other therapeutic procedures. The mutations of the Gárdos channel are one among many disorders that lead to the dehydration of red blood cells causing a subtype of anemia known as Hereditary Xerocytosis. The disease is treated with several inhibitors such as antimycotic clotrimazole[47] and TRAM-34 [53]. However, their inability to target all three mutations i.e., R352H, V282E, and V282M [44], causes a hindrance in their selectivity profile. Moreover, most of the research done on the Gárdos Channel was in-vitro and in-vivo. The structure of the Gárdos channel was published in 2018 [39]. There were structural limitations for employing computational research on the Gárdos channel and there was no mutant structure available for the channel. Due to the lack of sufficient data in previous studies, a limited number of ligand dataset was obtained from ChEMBL, with the use of the existing crystal structure, the mutant structure of the Gárdos channel was modeled [52], consisting of the most common mutations known as R352H and the V282M. The publication of the cyro-EM structure of the Gárdos channel facilitated the way toward predictions. Predictions are always recommended for computational experiments to reduce the time and cost [54].

The data of known ligands and mutant models of the Gardos Channel was obtained from Literature [52]. This present study added value to previous research by searching out modulators of the Gardos Channel utilizing computational methods. Using the known data from the literature, ligand-based pharmacophore models were developed. Utilizing the pharmacophore models, virtual screening of the unknown drug data is done to filter out hits for the Gardos Channel. The same interactions were found around all the ligands and the GRIND analysis too provided features that were consistent with the docking output. The potent hits were docked, and the top docked pose was selected based on the highest fitness score. A molecular dynamic simulation of the selected complex was carried out to check stability [55]. The current study aided in the development of drugs effective against all three types of mutations in the Gardos Channel, aiding in the control of diseases associated with the channel such as sickle cell anemia [23], hereditary spherocytosis [5], and hereditary elliptocytosis[17].

Chapter 6

Conclusion

Conclusion

The hereditary mutations in the Gardos Channel make the channel less sensitive to Ca^{2+} , allowing a lesser concentration of Ca^{2+} to open the channel and lead towards pathogenicity. The present research utilized a computational drug design approach for the virtual screening of modulators of the Gardos Channel. Ligand-based pharmacophore models were developed. Model 1 was generated using an efficient tool Ligandscout which develops models based on similar features in between compounds. The model was developed with four common features which are HBA, H1, H2 and Aromatic. These features' distances are HBA - H1 feature at a distance of 3.66Å, HBA - Aromatic feature at a distance of 3.34Å, HBA - H2 feature at a distance of 4.6Å, H1 - Aromatic feature at a distance of 0.33Å, H1 - H2 feature at a distance of 5.91Å and Aromatic - H2 feature at a distance of 5.67Å. Model 2 was developed by software Molecular Operating Environment version 2015. The highest active ligand from known data was selected for template. Five active features were selected of template which are F1 Aromatic and Hydrophobic, F2 Aromatic and Hydrophobic, F3 Aromatic and Hydrophobic, HBA and HBD. The distances between features are F1 Aromatic and Hydrophobic - F2 Aromatic and Hydrophobic features at a distance 5.16Å, F1 Aromatic and Hydrophobic - F3 Aromatic and Hydrophobic feature at a distance 4.85Å, F1 Aromatic and Hydrophobic - HBA feature at a distance 4.07Å, F1 Aromatic and Hydrophobic - HBD feature at a distance 5.36Å, F2 Aromatic and Hydrophobic - F3 Aromatic and Hydrophobic feature at a distance 5.29Å, F2 Aromatic and Hydrophobic - HBA feature at a distance 4.89Å, F2 Aromatic and Hydrophobic - HBD feature at a distance 3.78Å, F3 Aromatic and Hydrophobic - HBA feature at a distance 4.67Å, F3 Aromatic and Hydrophobic - HBD feature at a distance 4.38Å and HBA - HBD feature at a distance 2.23Å. Both models were evaluated with a defined threshold of active and inactive from known data. Model 2 outperformed Model 1 in the evaluation of precision metrics, so the protocol moved forward with model 2. Virtual screening was carried out of unknown drug data retrieved from the ChemBridge database. A total of 312 hits were selected by model. GRIND analysis was applied on hits to predict their IC_{50} . The use of Molecular Docking and Molecular Dynamic simulation along with pharmacophore-based virtual screening significantly enhance the precision of predictions. The top 10 compounds with high IC_{50} were docked at the Calmodulin binding domain and the same interactions were observed as in the literature. The top pose was simulated to probe the stability of the complex. The molecular dynamics simulations result showed the presence of residues MET282, ALA297, THR278, TYR199, LEU198 and VAL195 within vicinity of ligand. The presence of MET282 and ALA297 is

important as they formed a hydrophobic pocket, thus providing optimal fit of ligand and MET282 is one of our target mutations. This compound exhibits superior interactions with the target, as no previously identified ligand has demonstrated interactions with the specific point mutation. The predicted IC_{50} of this compound is 5.85nM while the IC_{50} of the top active compound from known data is 8.99nM, so therefore, it has better binding potential against the Gardos channel than the already known compounds. The Lipophilic efficiency value of this compound is 7.47 which qualify the FDA criteria of an average oral drug which further strengthen our lead.

As future aspect, we propose these top hits selected by our model for mutagenesis studies. Therefore, the present research can be an asset in the in-silico analysis and the design of new drugs.

Chapter 7

References

References

1. Vichinsky, E., *New therapies in sickle cell disease*. The Lancet, 2002. **360**(9333): p. 629-631.
2. Ataga, K.I. and J. Stocker, *The trials and hopes for drug development in sickle cell disease*. British Journal of Haematology, 2015. **170**(6): p. 768-780.
3. Vrontaki, E., et al., *Exploiting ChEMBL database to identify indole analogs as HCV replication inhibitors*. Methods, 2015. **71**: p. 4-13.
4. Stuart, J., et al., *Additive in vitro effects of anti-sickling drugs*. British journal of haematology, 1994. **86**(4): p. 820-823.
5. Archer, N.M., et al., *Hereditary xerocytosis revisited*. Am J Hematol, 2014. **89**(12): p. 1142-6.
6. Andolfo, I., et al., *Novel Gardos channel mutations linked to dehydrated hereditary stomatocytosis (xerocytosis)*. American journal of hematology, 2015. **90**(10): p. 921-926.
7. Vandorpe, D.H., et al., *cDNA Cloning and Functional Characterization of the Mouse Ca²⁺-gated K⁺ Channel, mIK1: ROLES IN REGULATORY VOLUME DECREASE AND ERYTHROID DIFFERENTIATION**. Journal of Biological Chemistry, 1998. **273**(34): p. 21542-21553.
8. Doyle, D.A., et al., *The Structure of the Potassium Channel: Molecular Basis of K⁺ Conduction and Selectivity*. Science, 1998. **280**(5360): p. 69-77.
9. Vuorinen, A. and D. Schuster, *Methods for generating and applying pharmacophore models as virtual screening filters and for bioactivity profiling*. Methods, 2015. **71**: p. 113-134.
10. Hoffman, J.F., et al., *The hSK4 (KCNN4) isoform is the Ca²⁺-activated K⁺ channel (Gardos channel) in human red blood cells*. Proceedings of the National Academy of Sciences, 2003. **100**(12): p. 7366-7371.
11. Ishii, T.M., et al., *A human intermediate conductance calcium-activated potassium channel*. Proceedings of the National Academy of Sciences, 1997. **94**(21): p. 11651-11656.
12. De Franceschi, L., et al., *Evidence for a protective role of the Gardos channel against hemolysis in murine spherocytosis*. Blood, 2005. **106**(4): p. 1454-1459.
13. Wiley, J.S., *Inherited red cell dehydration: a hemolytic syndrome in search of a name*. Pathology, 1984. **16**(2): p. 115-6.
14. Ghatta, S., et al., *Large-conductance, calcium-activated potassium channels: structural and functional implications*. Pharmacology & therapeutics, 2006. **110**(1): p. 103-116.
15. Kucherenko, Y.V., et al., *Effect of chloride channel inhibitors on cytosolic Ca²⁺ levels and Ca²⁺-activated K⁺(Gardos) channel activity in human red blood cells*. The Journal of membrane biology, 2013. **246**: p. 315-326.
16. Gilli, R., et al., *Thermodynamic Analysis of Calcium and Magnesium Binding to Calmodulin*. Biochemistry, 1998. **37**(16): p. 5450-5456.
17. Kilhoffer, M.-C., et al., *The heterodimer calmodulin: myosin light-chain kinase as a prototype vertebrate calcium signal transduction complex*. Biochimica et Biophysica Acta (BBA) - Protein Structure and Molecular Enzymology, 1992. **1160**(1): p. 8-15.
18. Morales, P., et al., *Contribution of the KCa3.1 channel-calmodulin interactions to the regulation of the KCa3.1 gating process*. J Gen Physiol, 2013. **142**(1): p. 37-60.
19. Garneau, L., et al., *Hydrophobic interactions as key determinants to the KCa3.1 channel closed configuration. An analysis of KCa3.1 mutants constitutively active in zero Ca²⁺*. J Biol Chem, 2009. **284**(1): p. 389-403.

20. Klein, H., et al., *Structural determinants of the closed KCa3.1 channel pore in relation to channel gating: results from a substituted cysteine accessibility analysis*. J Gen Physiol, 2007. **129**(4): p. 299-315.
21. Gallagher, P.G., *Disorders of erythrocyte hydration*. Blood, The Journal of the American Society of Hematology, 2017. **130**(25): p. 2699-2708.
22. Caulier, A., et al., *Primary red cell hydration disorders: pathogenesis and diagnosis*. International journal of laboratory hematology, 2018. **40**: p. 68-73.
23. Fermo, E., et al., *'Gardos Channelopathy': a variant of hereditary Stomatocytosis with complex molecular regulation*. Scientific Reports, 2017. **7**(1): p. 1744.
24. Chou, C.C., C.A. Lunn, and N.J. Murgolo, *KCa3.1: target and marker for cancer, autoimmune disorder and vascular inflammation?* Expert Rev Mol Diagn, 2008. **8**(2): p. 179-87.
25. Jäger, H., et al., *Blockage of intermediate-conductance Ca²⁺-activated K⁺ channels inhibit human pancreatic cancer cell growth in vitro*. Mol Pharmacol, 2004. **65**(3): p. 630-8.
26. Grgic, I., et al., *Renal fibrosis is attenuated by targeted disruption of KCa3.1 potassium channels*. Proc Natl Acad Sci U S A, 2009. **106**(34): p. 14518-23.
27. Huang, C., C.A. Pollock, and X.M. Chen, *KCa3.1: a new player in progressive kidney disease*. Curr Opin Nephrol Hypertens, 2015. **24**(1): p. 61-6.
28. Wulff, H. and N.A. Castle, *Therapeutic potential of KCa3.1 blockers: recent advances and promising trends*. Expert Rev Clin Pharmacol, 2010. **3**(3): p. 385-96.
29. Toyama, K., et al., *The intermediate-conductance calcium-activated potassium channel KCa3.1 contributes to atherogenesis in mice and humans*. J Clin Invest, 2008. **118**(9): p. 3025-37.
30. Romero, J.R., et al., *Arginine supplementation of sickle transgenic mice reduces red cell density and Gardos channel activity*. Blood, The Journal of the American Society of Hematology, 2002. **99**(4): p. 1103-1108.
31. Jansen, J., et al., *Mechanistic ion channel interactions in red cells of patients with Gárdos channelopathy*. Blood Advances, 2021. **5**(17): p. 3303-3308.
32. Horvath, D., *Pharmacophore-based virtual screening*. Chemoinformatics and computational chemical biology, 2011: p. 261-298.
33. Kaestner, L., A. Bogdanova, and S. Egee, *Calcium channels and calcium-regulated channels in human red blood cells*. Calcium signaling, 2020: p. 625-648.
34. Picard, V., et al., *Rapid Gardos Hereditary Xerocytosis Diagnosis in 8 Families Using Reticulocyte Indices*. Frontiers in Physiology, 2021. **11**: p. 602109.
35. Rapetti-Mauss, R., et al., *A mutation in the Gardos channel is associated with hereditary xerocytosis*. Blood, 2015. **126**(11): p. 1273-1280.
36. Petkova-Kirova, P., et al., *The Gárdos Channel and Piezo1 Revisited: Comparison between Reticulocytes and Mature Red Blood Cells*. 2023.
37. Ali, M.A., et al., *Efficacy and safety of recently approved drugs for sickle cell disease: a review of clinical trials*. Experimental hematology, 2020. **92**: p. 11-18. e1.
38. Glasel, J.A., et al., *Potassium channels: gene family, therapeutic relevance, high-throughput screening technologies and drug discovery*. Progress in drug research, 2002: p. 133-168.
39. Lee, C.-H. and R. MacKinnon, *Activation mechanism of a human SK-calmodulin channel complex elucidated by cryo-EM structures*. Science, 2018. **360**(6388): p. 508-513.
40. Schumacher, M.A., et al., *Structure of the gating domain of a Ca²⁺-activated K⁺ channel complexed with Ca²⁺/calmodulin*. Nature, 2001. **410**(6832): p. 1120-1124.

41. Orfali, R., et al., *Channelopathy-causing mutations in the S45A/S45B and HA/HB helices of KCa2. 3 and KCa3. 1 channels alter their apparent Ca²⁺ sensitivity*. Cell Calcium, 2022. **102**: p. 102538.
42. Brugnara, C., et al., *Therapy with oral clotrimazole induces inhibition of the Gardos channel and reduction of erythrocyte dehydration in patients with sickle cell disease*. The Journal of clinical investigation, 1996. **97**(5): p. 1227-1234.
43. Orfali, R. and N. Albanyan, *Ca²⁺-Sensitive Potassium Channels*. Molecules, 2023. **28**(2): p. 885.
44. Glogowska, E., et al., *Mutations in the Gardos channel (KCNN4) are associated with hereditary xerocytosis*. Blood, 2015. **126**(11): p. 1281-1284.
45. Lew, V.L., et al., *Distribution of dehydration rates generated by maximal Gardos-channel activation in normal and sickle red blood cells*. Blood, 2005. **105**(1): p. 361-367.
46. Rivera, A., et al., *The erythroid K-Cl cotransport inhibitor [(dihydroindenyl) oxy] acetic acid blocks erythroid Ca²⁺-activated K⁺ channel KCNN4*. American Journal of Physiology-Cell Physiology, 2022. **323**(3): p. C694-C705.
47. Ataga, K.I. and J. Stocker, *Senicapoc (ICA-17043): a potential therapy for the prevention and treatment of hemolysis-associated complications in sickle cell anemia*. Expert Opin Investig Drugs, 2009. **18**(2): p. 231-9.
48. Tubman, V.N., et al., *The clinically tested gardos channel inhibitor senicapoc exhibits antimalarial activity*. Antimicrobial Agents and Chemotherapy, 2016. **60**(1): p. 613-616.
49. Maher, A.D. and P.W. Kuchel, *The Gárdos channel: a review of the Ca²⁺-activated K⁺ channel in human erythrocytes*. The International Journal of Biochemistry & Cell Biology, 2003. **35**(8): p. 1182-1197.
50. Ellory, J.C., et al., *Mode of action and comparative efficacy of pharmacological agents that inhibit calcium-dependent dehydration of sickle cells*. (0007-1188 (Print)).
51. Agrawal, R.K., et al., *Hydroxyurea in sickle cell disease: drug review*. Indian J Hematol Blood Transfus, 2014. **30**(2): p. 91-6.
52. Ahmad, M., *Combined Structure and Ligand Guided Protocols to Target the Gain-of-function Mutation of Gárdos Channel in Red Cell Deformability*. 2021, National University of Sciences and Technology Islamabad.
53. Agarwal, J.J., et al., *TRAM-34, a putatively selective blocker of intermediate-conductance, calcium-activated potassium channels, inhibits cytochrome P450 activity*. PLoS One, 2013. **8**(5): p. e63028.
54. Hollingsworth, S.A. and R.O. Dror, *Molecular dynamics simulation for all*. Neuron, 2018. **99**(6): p. 1129-1143.
55. Hansson, T., C. Oostenbrink, and W. van Gunsteren, *Molecular dynamics simulations*. Current opinion in structural biology, 2002. **12**(2): p. 190-196.